Theor Chem Acc (2011) 128:83–90
DOI 10.1007/s00214-010-0765-z

REGULAR ARTICLE

Quantum mechanical/molecular mechanical study of anthrax lethal factor catalysis

Christopher R. Smith · Gregory K. Smith · Zhenxiao Yang · Dingguo Xu · Hua Guo

Received: 26 March 2010 / Accepted: 5 May 2010 / Published online: 22 May 2010

Abstract We report a hybrid quantum mechanical and molecular mechanical study of the catalysis of anthrax lethal factor. The calculations suggest that the zinc peptidase uses the same general base-general acid mechanism as in thermolysin and carboxypeptidase A, in which a zinc-bound water is activated by Glu687 to nucleophilically attack the scissile carbonyl carbon in the substrate. The catalysis is aided by an oxyanion hole formed by the zinc ion and the side chain of Tyr728, which provide stabilization for the fractionally charged carbonyl oxygen. The assigned role of Tyr728 differs from previous suggestions but is consistent with the established mechanism of other zinc proteases.

Keywords QM/MM · Lethal factor · Enzyme · Catalysis

1 Introduction

Anthrax is an infection of humans and animals caused by the Gram-positive bacterium *Bacillus anthracis*. Although anthrax is one of the oldest diseases known to man, it has recently attracted renewed attention because of its potential as an agent for bioterrorism and biological warfare [1]. This bacterium has the ability to form spores, which can lay dormant for decades even under unfavorable conditions. Infections occur when the bacterial spores enter the host via lacerations, ingestion, or inhalation. While the most common cutaneous anthrax is curable, systemic infection via inhalation is significantly more dangerous, leading to host death within days without treatment, and significant mortality rates even with early intervention [2]. The inhaled spores germinate in alveolar macrophages and are carried to the lymph nodes where they multiply and enter the bloodstream in mass. The vegetative bacteria then release several virulence factors, causing massive toxemia that leads to eventual host death. Due to the circulation of virulence factors, antibiotics are only effective if started early, and any late-stage treatments must address the circulating toxins as well. The difficulties in diagnosis coupled with the short time window available to take effective action make anthrax a potent threat.

The primary virulence factors of *B. anthracis* include a protective capsule that inhibits phagocytosis and three polypeptides: protective antigen (PA), edema factor (EF), and lethal factor (LF) [3]. The peptides work in concert as two binary toxins, as PA binds to surface anthrax toxin receptors (ATR) and facilitates entry of either EF or LF into the cytosol. EF is a calcium and calmodulin-dependent adenylate cyclase that raises cAMP concentrations within the cell, leading to edema. The more potent of the two is LF, a zinc-dependent protease that targets mitogen-activated protein kinase kinase (MAP2K). Its central role in mortality has been demonstrated in animal studies, which show injection of lethal toxin (LF + PA) leads to similar progression as the bacterial infection [1].

The LF is a four domain ~90 kDa protease with a zinc cofactor and consensus zinc-binding motif HEXXH [4].

C. R. Smith · G. K. Smith · H. Guo (✉)
Department of Chemistry and Chemical Biology,
University of New Mexico, Albuquerque, NM 87131, USA
e-mail: hguo@unm.edu

Z. Yang
National Institute of Biological Sciences, 102206 Beijing, China

D. Xu
MOE Key Laboratory of Green Chemistry and Technology,
College of Chemistry, Sichuan University, 610064 Chengdu,
Sichuan, China

This highly specific metalloprotease cleaves the amide bond in MAP2Ks near their N termini [5–10]. Although the exact mechanism of the resulting cell death is still unclear, it is understood that the cleavage of MAP2K disrupts downstream processes, which are responsible for activating host immunological and inflammatory responses [11]. Given its central role in anthrax infections, LF offers an important target for designing therapeutic agents [12]. Although some successes have been reported [13–18], it is apparent that further advancement will benefit from better understanding of the substrate binding and catalysis of LF.

There have been a number of kinetic studies of the LF catalysis [19, 20], which reported K_m and k_{cat} values for various substrates. X-ray structures of LF have also been reported in its apo form [21] and complexed with substrates [14, 21] and inhibitors [13, 15–17]. Apart from the hallmark HEXXH motif, the catalytic domain (IV) of LF has no sequence homology with any other known proteins, but its backbone scaffold resembles closely that of thermolysin [21]. Figure 1 shows the X-ray structure of LF complexed with a peptide substrate (LF20) [14].

It is now well established that the zinc cofactor in the catalytic domain is coordinated at the bottom of the active site cleft by three protein ligands: His686, His690, Glu735, and a water molecule [21]. Mutations of zinc-binding residues completely abolish the activity of LF [4, 22, 23]. Near the metal center, there are two important second-shell residues: Glu687 and Tyr728 (see Scheme 1). The LF active site is quite analogous to the much more extensively studied thermolysin [24] and carboxypeptidase A [25], and a similar catalytic mechanism has been proposed [21]. This entails Glu687 serving as the general base to activate a zinc-bound water, which attacks the scissile amide bond. Mutation of Glu687 to Cys has been found to completely inactivate LF [4, 22]. The role of the nearby Tyr728 is more controversial. It was initially suggested based on the crystallographic structure of the apo LF that it may serve as a general acid to protonate the amine leaving group [21]. Later, Tonello et al. [23] found that its mutation to Phe results in the complete abolishment of activity, and these authors proposed that the Tyr residue might be involved in stabilizing the leaving amide group of the substrate. However, it is also possible that it serves as part of the oxyanion hole to stabilize the negative charge developed at the carbonyl oxygen atom [12], a role played by His231 in thermolysin and Arg127 in carboxypeptidase A.

There have been few computational investigations into LF, and none has investigated its catalysis. Johnson et al. [26] presented in 2006 a structure–activity relationship (SAR) study of several inhibitors of LF. More recently, Hong et al. [27] studied the Michaelis complex using density functional theory (DFT) and molecular dynamics (MD). Convincing evidence was shown that the zinc-bound nucleophile is a neutral water, rather than hydroxide, and it forms a hydrogen bond with the putative general base Glu687 [27]. The interaction of LF with several MAPK/ERK and MAP2K substrates was also investigated recently by Dalkas et al. [28], using docking and MD simulations. Both MD simulations have relied on force fields in describing the Zn(II)-ligand binding. Here, we report a theoretical investigation into the catalysis of LF. In particular, we studied the Michaelis complex as well as catalysis of the wild type and Y728F mutant using a quantum mechanical/molecular mechanical (QM/MM) approach. These studies allowed a better understanding of the LF catalysis.

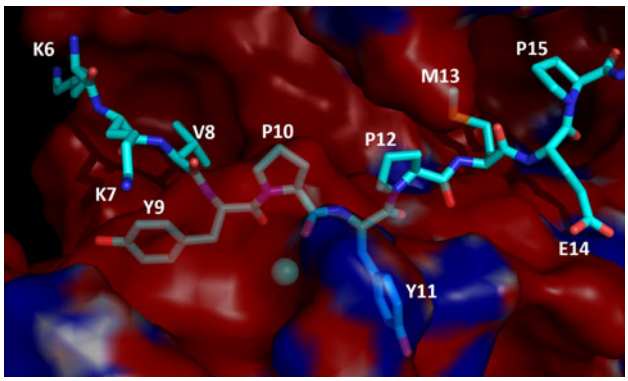

Fig. 1 The X-ray structure of anthrax lethal factor complexed with the LF20 peptide (PDB code 1PWW) [14]. The protein surface is colored by the solvent accessible potential map, where *blue* represents areas of negative potential, *red* positive, and *white* neutral. LF20 is shown in *stick* representation, where carbon is *light blue*, nitrogen *dark blue*, and oxygen is *red*

2 Methods

2.1 Model

The starting point of the simulation was selected from an enzyme–substrate complex structure (PDB code 1PWW) [14], which is a point mutation (E687C) of LF complexed

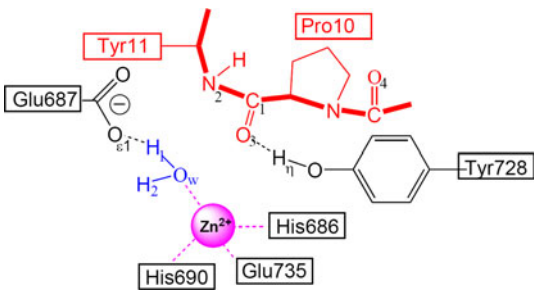

Scheme 1 Arrangement of the active site of the anthrax lethal factor and atom definition. The substrate is coded *red,* while the nucleophilic water is coded *blue*

with an optimized synthetic substrate (LF20). This structure was chosen because it represented the ES complex that showed the least amount of deformation after mutation and bound the substrate in what appeared to be a productive conformation. Note that the substrate in this LF complex is not a member of the MAP2K family. Rather, it is an analog with a consensus sequence $M_1L_2A_3R_4R_5K_6K_7V_8Y_9$-$P_{10}Y_{11}P_{12}M_{13}E_{14}P_{15}T_{16}I_{17}A_{18}E_{19}G_{20}$-amide, in which the amide bond between Y_9 and P_{10} represents the cleavage site. In the X-ray structure, only the residues between K_6 and E_{14} in this substrate were resolved, and no attempt was made in our simulations to extend it to its full length. The 1PWW structure was also used by Hong et al. [27] in their recent MD simulations of LF. The earlier structure reported by Pannifer et al. [21] was also examined but not used due to the fact that the substrate was bound in a non-productive conformation, and a $\sim 180°$ turn of the peptide chain is required to bring it to the correct binding mode. Such non-productive binding of substrates is known to be kinetically viable [19].

The X-ray structure was modified by recovering the Glu687 side chain in silico. A water molecule was then added to the active site close to the metal ion. Hydrogen atoms were added using the HBUILD utility in CHARMM [29], and the titratable residues in the enzyme were assigned the appropriate ionization states at pH = 7. In particular, the histidine residues took the following ionization states: HSD (H on $N_{\delta 1}$) for residues 42, 117, 197, 229, 424, 645, 654, 669, 686, 690, and 745, while HSE (H on $N_{\varepsilon 2}$) for residues 35, 91, 115, 277, 280, 309, 588, and 749. The resulting structure was then solvated by a pre-equilibrated sphere of TIP3P waters [30] with 25 Å radius centered at the zinc ion, followed by a 10 ps MD simulation with all protein and substrate atoms fixed. This process was repeated twice with randomly rotated water spheres to ensure uniform solvation.

To reduce computational costs, stochastic boundary conditions were employed [31]. To this end, atoms outside the 25 Å radius were removed, while atoms in the buffer zone (22 Å $< r <$ 25 Å) were subjected to harmonic restraining potentials. In the inner reaction region ($r <$ 22 Å), the motion of atoms is governed by the QM/MM potential. A group-based switching scheme was used for non-bonded interactions [32]. The MD simulations feature Newtonian dynamics for atoms in the reaction zone, augmented by Langevin dynamics of atoms in the buffer region at 300 K.

2.2 Quantum mechanical/molecular mechanical

The combined quantum mechanical and molecular mechanical (QM/MM) approach [33] has been extensively applied to study enzymatic systems [34–39]. Such a method has the advantage that a very large system such as an enzyme can be investigated with manageable computation costs. The basic idea of the QM/MM scheme is to divide the system into two parts: the smaller QM region where the chemical bond breaking and forming take place is treated with quantum mechanics, while the surrounding region is described by a MM force field.

In this work, the QM region was characterized by the self-consistent charge-density functional tight binding (SCC-DFTB) model [40] and the MM region by the CHARMM all atom force field [41]. SCC-DFTB is an approximate DFT method and it is much more efficient than ab initio QM/MM approaches. The efficiency is essential for metallo-enzymes because the active site is often much too large for an accurate ab initio QM/MM free-energy simulation. The SCC-DFTB model has been extensively tested for enzyme systems [37, 42–44] including those with zinc cofactors [45]. Its accuracy is comparable to the commonly used AM1 and PM3 [43, 44]. The QM/MM approach based on the SCC-DFTB method has been shown to give a reasonable description of several zinc enzymes including carbonic anhydrase [46, 47] β-lactamases [48–52], cytidine deaminase [53], and carboxypeptidase A [54]. On the other hand, we also note that SCC-DFTB is not appropriate for all situations, such as was reported for the ligand binding energy of Zn(II) [55]. However, complete dissociation is not relevant here, and we expect the impact of this imperfection to be minimal for near equilibrium properties.

All simulations were performed with CHARMM (version 32a2) with a SCC-DFTB interface [42]. The QM region includes the side chains of His686, His690, Glu687, Glu735, and Tyr728; all atoms of Pro_{10} and the backbone atoms of Tyr_9 and Tyr_{11} from the substrate; the catalytic water; and the zinc ion. At the boundary, the link atom (QQ) approach [56] was used. All mutants were treated in a similar fashion.

In the QM/MM MD simulation of the Michaelis complex, the starting system was brought to 300 K in 50 ps, followed by 150 ps of equilibration. The final 800 ps MD trajectory was used for analysis. The MD trajectories were integrated with a 1.0 fs time interval, and the SHAKE algorithm [57] was used to maintain all covalent bonds involving hydrogen atoms.

Minimal energy paths were calculated using adiabatic mapping along two putative reaction coordinates. For the nucleophilic addition (NA) of the water nucleophile, the reaction coordinate is given by the distance between the water oxygen (O_w) and the substrate carbonyl carbon (C_1): $r_1 = d_{O_w \cdots C_1}$. For the elimination (E) of the leaving group, the corresponding reaction coordinate is given by a combination of N_2–H_1 and C_1–N_2 distances: $r_2 = d_{N_2 \cdots H_1} - d_{C_1 \cdots N_2}$.

2.3 Potential of mean force

The minimum energy structures along a putative reaction coordinate were used as the initial points for calculating the potential of mean force (PMF). The PMF calculations used umbrella sampling [58] with harmonic constraints of 100–400 kcal/mol Å^2. At least twenty windows were used for the NA and E steps. In each window, a 50 ps equilibration simulation was first performed to bring the system to 300 K. The distribution function in the reaction coordinate was then collected in the subsequent 100 ps. The final PMF was obtained using the weighted histogram analysis method (WHAM) [59].

3 Results

The 1.0 ns MD simulation indicated that the enzyme–substrate (ES) complex is reasonably stable, as evidenced by the RMSD (root mean square deviation) shown in Fig. 2. The averaged values of several key internuclear distances are given in Table 1. In the ES complex, the substrate is tightly held by both electrostatic and hydrophobic interactions. As previously noted [14], two upstream residues at the P4 and P5 positions (Lys_7 and Lys_6) of the substrate are locked in strong electrostatic interaction with negatively charged residues of LF including Asp647 and Glu733. Also note the P2 (Tyr_9) and P1′ (Tyr_{11}) residues have their phenyl rings inserting into hydrophobic cavities, as shown in Fig. 1.

In the active site of the ES complex, the water serves as the fourth ligand to Zn(II), in addition to His686, His690, and Glu735. The O_w–Zn distance of 2.03 ± 0.06 Å, typical for a neutral oxygen ligand, is consistent with the experimental value of 2.10 ± 0.1 Å [21]. As in X-ray structures [14, 21], the carboxylate-Zn coordination for Glu735 is monodentate. However, multiple rotations of the carboxylate have been observed in the MD simulation, resulting in the switching of the coordination oxygen.

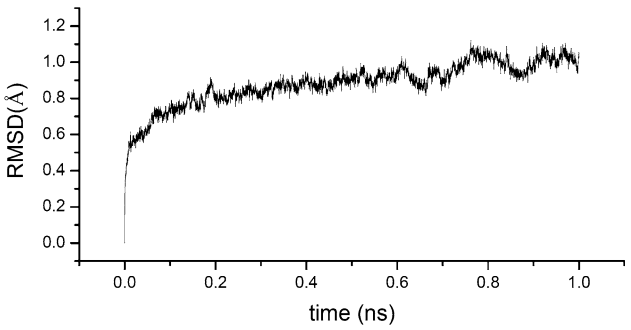

Fig. 2 RMSD for backbone atoms obtained in the QM/MM MD simulation of the ES complex

Table 1 Some key distances obtained from QM/MM MD simulations of the ES complex of the wild type LF and from QM/MM reaction path calculations

Distance (Å)	MD	Reaction path				
	ES	ES	TS1	INT	TS2	EP
C_1–O_w	2.73 ± 0.22	2.90	1.79	1.50	1.42	1.29
O_w–H_1	1.10	1.07	1.28	1.66	2.21	2.35
$O_{\varepsilon 2}$–H_1	1.37 ± 0.07	1.43	1.15	1.02	1.08	1.91
$O_{\varepsilon 1}$–H_2	2.58 ± 0.25	2.57	2.73	2.92	2.34	1.13
C_1–O_3	1.24 ± 0.02	1.23	1.33	1.39	1.35	1.30
C_1–N_2	1.38 ± 0.02	1.38	1.43	1.47	1.79	2.24
N_2–H_1	3.25 ± 0.27	3.67	3.27	3.39	1.59	1.04
O_4–H_2	3.10 ± 0.63	1.88	1.78	1.72	1.83	3.05
O_3–H_η	1.97 ± 0.17	1.90	1.85	1.81	1.92	2.05
O_3–Zn	3.59 ± 0.35	2.92	2.12	2.07	2.11	2.11
O_w–Zn	2.03 ± 0.06	2.03	2.88	2.89	2.85	2.86
N(H690)–Zn	2.03 ± 0.06	2.03	2.03	2.05	2.02	2.00
N(H686)–Zn	2.02 ± 0.06	2.04	2.05	2.07	2.02	2.01
O(E735)–Zn	2.07 ± 0.07	2.04	2.07	2.07	2.02	2.02

Throughout the simulation, nonetheless, the coordination maintains monodentate, as evidenced by the averaged O–Zn distances for the zinc-bound oxygen of 2.07 ± 0.07 Å. The zinc-bound water molecule is strongly hydrogen bonded with the carboxylate side chain of Glu687, and it forms an occasional hydrogen bond with the backbone carbonyl oxygen of $Tyr_9(O_4)$ as well. As a result, the nucleophile is in a perfect near attack position, with an average distance of 2.73 ± 0.22 Å between O_w and the scissile carbonyl carbon (C_1). In addition, the scissile carbonyl oxygen (O_3) of the substrate forms a hydrogen bond with the hydroxyl hydrogen of the Tyr728 side chain, as evidenced by the O_3-H_η distance of 1.97 ± 0.17 Å. On the other hand, we found no evidence that the zinc-bound water interacts with the Tyr728, as suggested by the apo enzyme structure [21]. Interestingly, the carbonyl oxygen O_3 is not directly coordinated with Zn(II), and the distance between the two is 3.59 ± 0.35 Å. The configuration of the active site described above is similar to the recent MD simulation of LF by Hong et al. [27].

The catalyzed reaction is initiated by the attack of the water nucleophile at the scissile carbonyl carbon (C_1), which leads to the first transition state (TS1), as shown by the PMF in Fig. 3. This nucleophilic addition (NA) barrier features a concerted addition of the water oxygen (O_w) to the carbonyl carbon (C_1) and the transfer of the water proton (H_1) to a carboxylate oxygen ($O_{\varepsilon 1}$) of the general base (Glu687), as suggested by the relevant internuclear distances listed in Table 1. The resulting tetrahedral intermediate (TI) is characterized by a sp^3 central carbon and protonated carboxylate side chain of Glu687. Due to

the negative charge developed on the scissile carbonyl oxygen (O_3) as a result of the OH^- addition, it replaces the water molecule as the fourth ligand of the zinc ion. As Fig. 3 shows, the PMF indicates that the TI is metastable and eventually collapses to the enzyme–product (EP) complex via the second transition state (TS2). This elimination (E) barrier features the elongation of the C_1–N_2 bond concomitant with the transfer of the proton from the Glu687 carboxylic acid to the leaving group nitrogen (N_2). The final EP complex contains the two cleaved peptide fragments, each bound to the active site by hydrogen bonds and augmented by Zn coordination. These two fragments eventually depart the active site to be replaced by solvent water. The general base Glu687 then recovers its ionization state and becomes ready for the next catalytic cycle. Throughout the reaction, the Zn coordination with the three protein ligands is maintained. Snapshots of the stationary points are displayed in Fig. 4, and the proposed catalytic mechanism is illustrated in Scheme 2.

For the wild type (WT), calculated free-energy barriers for the NA and E steps are 13.6 and 13.5 kcal/mol, respectively. Unfortunately, no kinetic data are available for the substrate LF20. However, the k_{cat} value (3.4 s^{-1}) has been measured for LF15 [14], which is closely related to LP20. The corresponding barrier height is 16.7 kcal/mol, as calculated using transition-state theory. It appears that the calculated barrier height underestimates the experimental value, which is consistent with past experiences with SCC-DFBT-based QM/MM methods [42, 51, 60]. We also note in passing that the barrier obtained in the reaction path for the first NA step is 25 kcal/mol. The lowering of the barrier by 11.4 kcal/mol underscores the relaxation of the system allowed by the room temperature MD simulation.

To gain more insights into the catalysis, we have also calculated the PMFs for the Y728F mutant, which has been studied experimentally [23]. The mutation removes the hydroxyl group in the side chain and thus the hydrogen bond with the carbonyl oxygen (O_3). The NA PMFs for the mutant is compared in Fig. 3 with that of the WT enzyme. It is clearly seen from the figure that the removal of the hydrogen bond with the scissile carbonyl oxygen (O_3) in the Y728F mutant leads to a significant increase in the barrier. The calculated barrier height of 18.1 kcal/mol for the Y728F mutant is 4.5 kcal/mol higher than the WT, which translates to approximately four orders of magnitude reduction in the rate constant. This dramatic increase in barrier underscores the importance of this residue in the catalysis as a part of the oxyanion hole, which along with the Zn ion stabilizes the negative charge on the carbonyl oxygen (O_3). This calculation result is consistent with the experimental observation that this point mutation abolished the activity of LF [23].

4 Discussion

Despite different folds, the LF active site is remarkably similar to that of thermolysin (TLN) [24] and carboxypeptidase A (CPA) [25]. Like in LF, the two extensively studied peptidases have a single zinc cofactor, ligated by two His and one Glu residue. An active site Glu residue,

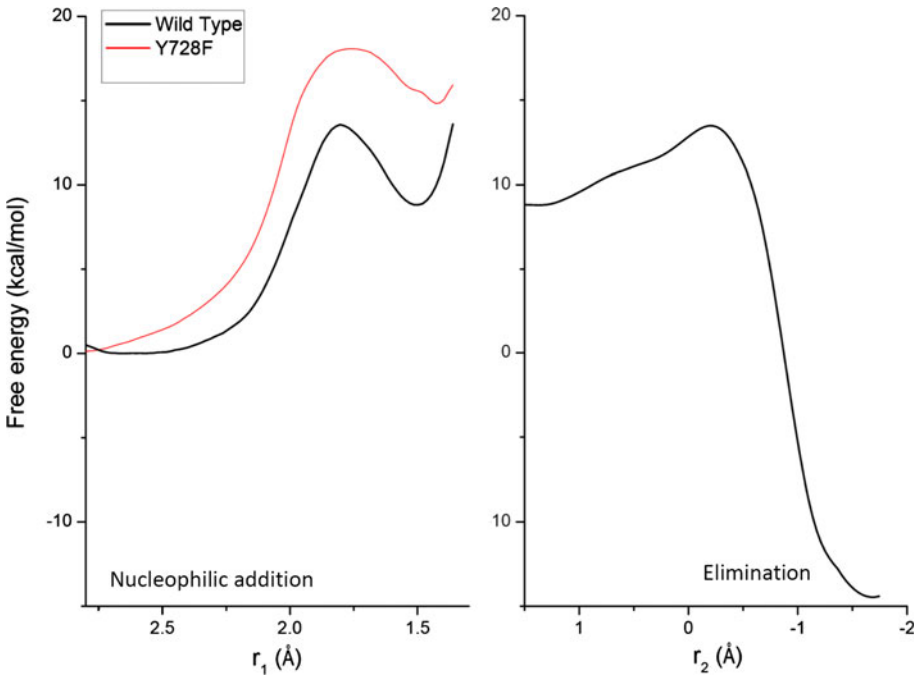

Fig. 3 Potentials of mean force (PMFs) for both the nucleophilic addition (NA) and elimination (E) steps of the hydrolysis reaction catalyzed by the wild type and Y728F mutant of the lethal factor. For the nucleophilic addition (NA) of the water nucleophile, the reaction coordinate is given by the distance between the water oxygen (O_w) and the substrate carbonyl carbon (C_1): $r_1 = d_{O_w \cdots C_1}$. For the elimination (E) of the leaving group, the corresponding reaction coordinate is given by a combination of N_2–H_1 and C_1–N_2 distances: $r_2 = d_{N_2 \cdots H_1} - d_{C_1 \cdots N_2}$

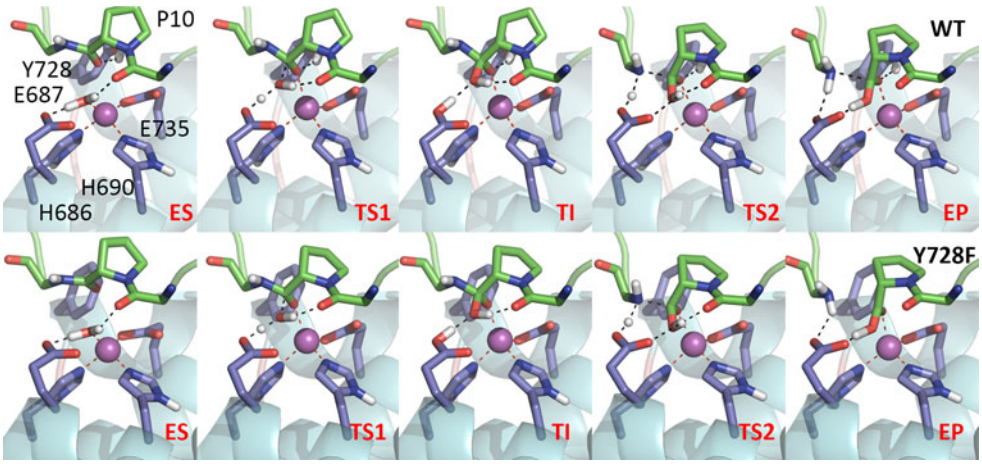

Fig. 4 Snapshots of the five stationary points along the reaction path for the wild type and Y728F mutant of the lethal factor. The *red dashed lines* indicate the ligand–metal bonds, while the *black dashed lines* represent either hydrogen bonds or partial bonds

Glu143 in TLN, and Glu270 in CPA serves as the general base in activating a zinc-bound water nucleophile. In addition, an active site residue provides hydrogen bonding to the scissile carbonyl oxygen. In TLN, it is His231, while in CPA, it is Arg127. Site-directed mutagenesis studies indicated that mutation of this residue resulted in significant reduction of the catalytic activity [61, 62]. Based on theoretical studies [54, 63], this residue contributes to both substrate binding as well as catalysis, serving as part of the oxyanion hole. This strategy is of course not restricted to these two well-studied zinc hydrolyases [64]. In histone deacetylase, for example, a second-shell Tyr residue is also found to stabilize the transition state [65]. Similarly, a Tyr residue was recently found to play an important catalytic role in dizinc lactonases [66].

Our PMF results reported here indicate that Tyr728 in LF serves the same role as His231 in TLN and Arg127 in CPA. Namely, it helps to bind the substrate and serves as part of the oxyanion hole to stabilize the negative charge developed in the carbonyl oxygen. These conclusions are at odds with the original proposal of Pannifer et al. [21], who suggested that Tyr728 serves as a proton donor to the nitrogen leaving group, and with that of Tonello et al. [23], who conjectured it as a stabilization for the leaving amino group. Our assigned role for Tyr728 is consistent with the mode of action in similar enzymes such as thermolysin and carboxypeptidase A, and with site-directed mutagenesis experiments on this residue [23].

Our simulations indicate that the catalytic role of the sole zinc cofactor in LF is to activate the water nucleophile and to provide stabilization for transition state via interaction with the negatively charged carbonyl oxygen. An interesting observation from our simulation is the weak interaction of the scissile carbonyl oxygen with Zn(II) in the ES complex, which suggests that the metal co-factor is not involved in the polarization of the substrate. These conclusions are in good agreement with the recent simulation of the thermolysin [63] and carboxypeptidase A [54]. As pointed out by Christianson and Lipscomb [25], direct zinc coordination by the peptide carbonyl leads to a non-productive binding mode, which displaces the nucleophilic water. Our results provide further supporting evidence for this argument.

5 Conclusions

The lethal factor is a key target for drug development specific to anthrax attack. In this work, we report a hybrid quantum mechanical/molecular mechanical study on the catalysis of the enzyme. The QM/MM approach provided for the first time a complete and detailed picture of the mode of action. Our results suggest that the catalyzed reaction follows a typical nucleophilic substitution reaction mechanism. The nucleophilic addition of the zinc-activated water to the scissile carbonyl carbon leads to a barrier featuring concurrent proton transfer to the general base Glu687. The resulting tetrahedral intermediate is stabilized by zinc coordination of the fractionally charged carbonyl oxygen and its hydrogen bond interaction with the hydroxyl group of Tyr728. The protonation of the leaving group nitrogen by the protonated carboxylate side chain of Glu687 eventually leads to the cleavage of the peptide bond.

Our model suggests that the Tyr728 residue, along with Zn(II), serves as the oxyanion hole in stabilizing the transition state, rather than protonating or stabilizing the nitrogen leaving group as suggested by previous authors.

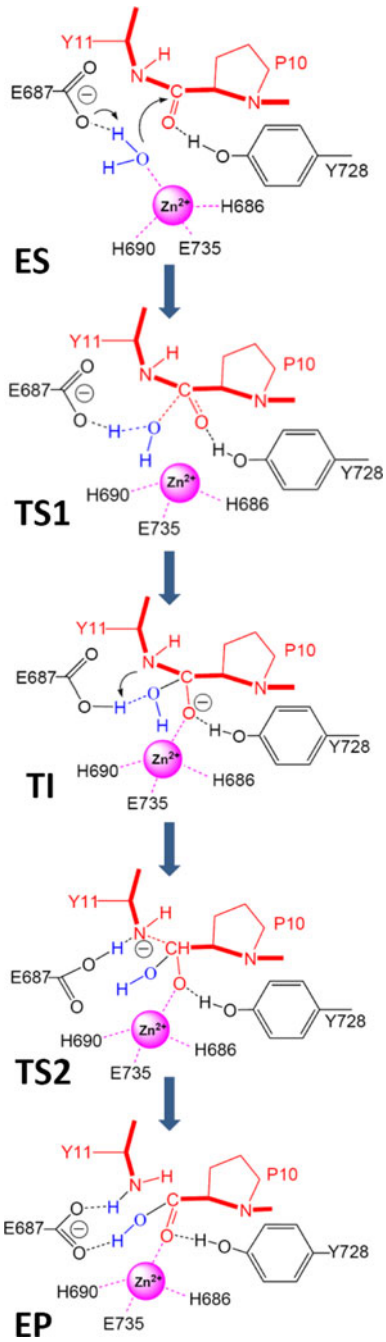

Scheme 2 Proposed catalytic mechanism of anthrax lethal factor based on the QM/MM calculations

Its contribution was assessed by the Y728F mutant, which indicates a significant increase in the barrier height. On the other hand, the zinc cofactor is found to play no role in polarizing the scissile carbonyl. These mechanistic details are consistent with the established mode of action in several zinc peptidases such as thermolysin and carboxypeptidase A, underscoring the power of convergent evolution. These similarities derive apparently from the analogous active site arrangement in these enzymes.

Acknowledgments This work at UNM was funded by the National Institutes of Health (R03-071992). GKS is a Nano-Science Micro-System (NSMS) IGERT fellow funded by the National Science Foundation. ZY is supported by Chinese Ministry of Science and Technology "863" Grant 2008AA022309. DX thanks the National Natural Science Foundation of China (No. 20803048) for partial support. Part of the calculations has been carried out at the National Center for Supercomputing Applications (NCSA). We thank Dr. F. Shao for numerous discussions on this system.

References

1. Bossi P, Garin D, Guihot A, Gay F, Crance J-M, Debord T, Autran B, Bricaire F (2006) Cell Mol Life Sci 63:2196–2212
2. Dixon TC, Meselson M, Guillemin J, Hanna PC (1999) N Engl J Med 341:815–826
3. Ascenzi P, Visca P, Ippolito G, Spallarossa A, Bolognesi M, Montecucco C (2002) FEBS Lett 531:384–388
4. Klimpel KR, Arora N, Leppla SH (1994) Mol Microbiol 13:1093–1100
5. Duesbery NS, Webb CP, Leppla SH, Gordon VM, Klimpel KR, Copeland TD, Ahn NG, Oskarsson MK, Fukasawa K, Paull KD, Vande Woude GF (1998) Science 280:734–737
6. Vitale G, Pellizzari R, Recchi C, Napolitani G, Mock M, Montecucco C (1998) Biochem Biophys Res Commun 248:706–711
7. Pellecchia M, Guidi-Rontani C, Vitale G, Mock M, Montecucco C (1999) FEBS Lett 462:199–204
8. Vitale G, Bernardi L, Napolitani G, Mock M, Montecucco C (2000) Biochem J 352:739–745
9. Park JM, Greten FR, Li Z-W, Karin M (2002) Science 297:2048–2051
10. Chopra AP, Boone SA, Liang X, Duesbery NS (2003) Proc Natl Acad Sci USA 278:9402–9406
11. Turk BE (2007) Biochem J 402:405–417
12. Turk BE (2008) Curr Pharm Biotechnol 9:24–33
13. Tonello F, Seveso M, Marin O, Mock M, Montecucco C (2002) Nature 418:386
14. Turk BE, Wong TY, Schwarzenbacher R, Jarrell ET, Leppla SH, Collier RJ, Liddington RC, Cantley LC (2004) Nat Struct Mol Biol 11:60–66
15. Panchal RG, Hermone AR, Nguyen TL, Wong TY, Schwarzenbacher R, Schmidt J, Lane D, McGrath C, Turk BE, Burnett J, Aman MJ, Little S, Sausville EA, Zaharevitz DW, Cantley LC, Liddington RC, Gussio R, Bavari S (2004) Nat Struct Mol Biol 11:67–72
16. Shoop WL, Xiong Y, Wiltsie J, Woods A, Guo J, Pivnichny JV, Felcetto T, Michael BF, Bansal A, Cummings RT, Cunningham BR, Friedlander AM, Douglas CM, Patel SB, Wisniewski D, Scapin G, Salowe SP, Zaller DM, Chapman KT, Scolnick EM, Schmatz DM, Bartizal K, MacCoss M, Hermes JD (2005) Proc Natl Acad Sci USA 102:7958–7963
17. Forino M, Johnson S, Wong TY, Rozanov DV, Savinov AY, Li W, Fattorusso R, Becattini B, Orry AJ, Jung D, Abagyan RA, Smith JW, Alibek K, Liddington RC, Strongin AY, Pellecchia M (2005) Proc Natl Acad Sci USA 102:9499–9504
18. Agrawal A, de Oliveria CAF, Cheng Y, Jacobsen JA, McCammon JA, Cohen SM (2009) J Med Chem 52:1063–1074
19. Tonello F, Ascenzi P, Montecucco C (2003) Proc Natl Acad Sci USA 278:40075–40078
20. Zakharova MY, Kuznetsov NA, Dubiley SA, Kozyr AV, Fedorova OS, Chudakov DM, Knorre DG, Shemyakin IG, Gabibov AG, Kolesnikov AV (2009) J Biol Chem 284:17902–17913
21. Pannifer AD, Wong TY, Schwarzenbacher R, Renatus M, Petosa C, Bienkowska J, Lacy DB, Collier RJ, Park S, Leppla SH, Hanna P, Liddington RC (2001) Nature 414:229–233

22. Hammond SE, Hanna PC (1998) Infect Immun 66:2374–2378
23. Tonello F, Naletto L, Romanello V, Dal Molin F, Montecucco C (2004) Biochem Biophys Res Commun 313:496–502
24. Matthews BW (1988) Acc Chem Res 21:333–340
25. Christianson DW, Lipscomb WN (1989) Acc Chem Res 22:62–69
26. Johnson SL, Jung D, Forino M, Chan Y, Satterthwait A, Rozanov DV, Strongin AY, Pellecchia M (2006) J Med Chem 49:27–30
27. Hong R, Magistrato A, Carloni P (2008) J Chem Theory Comput 4:1745
28. Dalkas GA, Papakyriakou A, Vlamis-Gardikas A, Spyroulias GA (2009) Protein Sci 18:1774–1785
29. Brooks BR, Bruccoleri RE, Olafson BD, States DJ, Swaminathan S, Karplus M (1983) J Comput Chem 4:187–217
30. Jorgensen WL, Chandrasekhar J, Madura JD, Impey RW, Klein ML (1983) J Chem Phys 79:926–935
31. Brooks CL III, Karplus M (1983) J Chem Phys 79:6312–6325
32. Steinbach PJ, Brooks BR (1994) J Comput Chem 15:667
33. Warshel A, Levitt M (1976) J Mol Biol 103:227–249
34. Gao J (1996) Methods and applications of combined quantum mechanical and molecular mechanical potentials. In: Lipkowitz KB, Boyd DB (eds) Reviews in computational chemistry, vol 7. VCH, New York, pp 119–185
35. Monard G, Merz KM Jr (1999) Acc Chem Res 32:904–911
36. Zhang Y (2006) Theor Chem Acc 116:43–50
37. Riccardi D, Schaefer P, Yang Y, Yu H, Ghosh N, Prat-Resina X, Konig P, Li G, Xu D, Guo H, Elstener M, Cui Q (2006) J Phys Chem B 110:6458–6469
38. Hu H, Yang W (2008) Annu Rev Phys Chem 59:573–601
39. Senn HM, Thiel W (2009) Angew Chem Int Ed 48:1198–1229
40. Elstner M, Porezag D, Jungnickel G, Elsner J, Haugk M, Frauenheim T, Suhai S, Seigert G (1998) Phys Rev B58:7260–7268
41. MacKerell AD Jr, Bashford D, Bellott M, Dunbrack RL Jr, Evanseck JD, Field MJ, Fischer S, Gao J, Guo H, Ha S, Joseph-McCarthy D, Kuchnir L, Kuczera K, Lau FTK, Mattos C, Michnick S, Ngo T, Nguyen DT, Prodhom B, Reiher WE III, Roux B, Schlenkrich M, Smith JC, Stote R, Straub J, Watanabe M, Wiorkiewicz-Kuczera J, Yin D, Karplus M (1998) J Phys Chem B 102:3586–3616
42. Cui Q, Elstner M, Kaxiras E, Frauenheim T, Karplus M (2001) J Phys Chem B 105:569–585
43. Sattelmeyer KW, Tirado-Rives J, Jorgensen WL (2006) J Phys Chem A 110:13551–13559
44. Otte N, Scholten M, Thiel W (2007) J Phys Chem A 111:5751–5755
45. Elstner M, Cui Q, Munih P, Kaxiras E, Frauenheim T, Karplus M (2003) J Comput Chem 24:565–581
46. Riccardi D, Cui Q (2007) J Phys Chem A 111:5703–5711
47. Riccardi D, Konig P, Guo H, Cui Q (2008) Biochemistry 47:2369–2378
48. Xu D, Zhou Y, Xie D, Guo H (2005) J Med Chem 48:6679–6689
49. Xu D, Xie D, Guo H (2006) J Biol Chem 281:8740–8747
50. Xu D, Guo H, Cui Q (2007) J Phys Chem A 111:5630–5636
51. Xu D, Guo H, Cui Q (2007) J Am Chem Soc 129:10814
52. Wang C, Guo H (2007) J Phys Chem B 111:9986–9992
53. Guo H, Rao N, Xu Q, Guo H (2005) J Am Chem Soc 127:3191–3197
54. Xu D, Guo H (2009) J Am Chem Soc 131:9780–9788
55. Amin EA, Truhlar DG (2008) J Chem Theory Comput 4:75–85
56. Field MJ, Bash PA, Karplus M (1990) J Comput Chem 11:700–733
57. Ryckaert JP, Ciccotti G, Berendsen HJ (1977) J Comput Phys 23:327–341
58. Torrie GM, Valleau JP (1977) J Comput Phys 23:187–199
59. Kumar S, Bouzida D, Swendsen RH, Kollman PA, Rosenberg JM (1992) J Comput Chem 13:1011–1021
60. Zhang X, Zhang X, Bruice TC (2005) Biochemistry 44:10443–10448
61. Phillips MA, Fletterick R, Rutter WJ (1990) J Biol Chem 265(33):20692–20698
62. Beaumont A, O'Donohue MJ, Paredes N, Rousselet N, Assicot M, Bohuon C, Fournie-Zaluski M-C, Roques BP (1995) J Biol Chem 270:16803–16808
63. Blumberger J, Lamoureux G, Klein ML (2007) J Chem Theory Comput 3:1837–1850
64. Lipscomb WM, Strater N (1996) Chem Rev 96:2375–2433
65. Corminboeuf C, Hu P, Tuckerman ME, Zhang Y (2006) J Am Chem Soc 128:4530–4531
66. Momb J, Wang C, Liu D, Thomas PW, Petsko GA, Guo H, Ringe D, Fast W (2008) Biochemistry 47:7715–7725